

### [Simulation of positron backscattering and implantation profiles using Geant4 code](#)

Huang Shi-Juan, Pan Zi-Wen, Liu Jian-Dang, Han Rong-Dian, Ye Bang-Jiao

Citation: Chin. Phys. B . 2015, 24(10): 107803. doi: 10.1088/1674-1056/24/10/107803

Journal homepage: <http://cpb.iphy.ac.cn>; <http://iopscience.iop.org/cpb>

What follows is a list of articles you may be interested in

---

### [Exploring positron characteristics utilizing two new positron-electron correlation schemes based on multiple electronic-structure calculation methods](#)

Zhang Wen-Shuai, Gu Bing-Chuan, Han Xiao-Xi, Liu Jian-Dang, Ye Bang-Jiao

Chin. Phys. B . 2015, 24(10): 107804. doi: 10.1088/1674-1056/24/10/107804

### [Effect of helium implantation on SiC and graphite](#)

Guo Hong-Yan, Ge Chang-Chun, Xia Min, Guo Li-Ping, Chen Ji-Hong, Yan Qing-Zhi

Chin. Phys. B . 2015, 24(3): 037803. doi: 10.1088/1674-1056/24/3/037803

### [A generalized method of converting CT image to PET linear attenuation coefficient distribution in PET/CT imaging](#)

Wang Lu, Wu Li-Wei, Wei Le, Gao Juan, Sun Cui-Li, Chai Pei, Li Dao-Wu

Chin. Phys. B . 2014, 23(2): 027802. doi: 10.1088/1674-1056/23/2/027802

### [Investigation of the free volume and ionic conducting mechanism of poly\(ethylene oxide\)-LiClO<sub>4</sub> polymeric electrolyte by positron annihilating lifetime spectroscopy](#)

Gong Jing, Gong Zhen-Li, Yan Xiao-Li, Gao Shu, Zhang Zhong-Liang, Wang Bo

Chin. Phys. B . 2012, 21(10): 107803. doi: 10.1088/1674-1056/21/10/107803

---

JUST FOR AUTHOR  
— CHINESE PHYSICS B

---

# 中国物理 **B**

# Chinese Physics **B**

Volume 24 Number 11 November 2015

Formerly *Chinese Physics*

---

A Series Journal of the Chinese Physical Society  
Distributed by IOP Publishing

---

Online: [iopscience.iop.org/cpb](http://iopscience.iop.org/cpb)  
[cpb.iphy.ac.cn](http://cpb.iphy.ac.cn)

---

CHINESE PHYSICAL SOCIETY  
**IOP** Publishing |

# Chinese Physics B

(First published in 1992)

Published monthly in hard copy by the Chinese Physical Society and online by IOP Publishing, Temple Circus, Temple Way, Bristol BS1 6HG, UK

## Institutional subscription information: 2015 volume

For all countries, except the United States, Canada and Central and South America, the subscription rate per annual volume is UK£974 (electronic only) or UK£1063 (print + electronic).

Delivery is by air-speeded mail from the United Kingdom.

### Orders to:

Journals Subscription Fulfilment, IOP Publishing, Temple Circus, Temple Way, Bristol BS1 6HG, UK  
For the United States, Canada and Central and South America, the subscription rate per annual volume is US\$1925 (electronic only) or US\$2100 (print + electronic). Delivery is by transatlantic airfreight and onward mailing.

### Orders to:

IOP Publishing, P. O. Box 320, Congers, NY 10920-0320, USA

© 2015 Chinese Physical Society and IOP Publishing Ltd

All rights reserved. No part of this publication may be reproduced, stored in a retrieval system, or transmitted in any form or by any means, electronic, mechanical, photocopying, recording or otherwise, without the prior written permission of the copyright owner.

Supported by the National Natural Science Foundation of China, the China Association for Science and Technology, and the Science Publication Foundation, Chinese Academy of Sciences

**Editorial Office:** Institute of Physics, Chinese Academy of Sciences, P. O. Box 603, Beijing 100190, China

Tel: (86-10) 82649026 or 82649519, Fax: (86-10) 82649027, E-mail: [cpb@aphy.iphy.ac.cn](mailto:cpb@aphy.iphy.ac.cn)

主管单位: 中国科学院

国际统一刊号: ISSN 1674-1056

主办单位: 中国物理学会和中国科学院物理研究所

国内统一刊号: CN 11-5639/O4

承办单位: 中国科学院物理研究所

编辑部地址: 北京 中关村 中国科学院物理研究所内

主 编: 欧阳钟灿

通 讯 地 址: 100190 北京 603 信箱

出 版: 中国物理学会

Chinese Physics B 编辑部

印刷装订: 北京科信印刷厂

电 话: (010) 82649026, 82649519

编 辑: Chinese Physics B 编辑部

传 真: (010) 82649027

国内发行: Chinese Physics B 出版发行部

“Chinese Physics B”网址:

国外发行: IOP Publishing Ltd

<http://cpb.iphy.ac.cn> (编辑部)

发行范围: 公开发行

<http://iopscience.iop.org/cpb> (IOPP)

## Published by the Chinese Physical Society

### 顾问 Advisory Board

陈佳洱 教授, 院士  
北京大学物理学院, 北京 100871

Prof. Academician Chen Jia-Er  
School of Physics, Peking University, Beijing 100871, China

冯 端 教授, 院士  
南京大学物理系, 南京 210093

Prof. Academician Feng Duan  
Department of Physics, Nanjing University, Nanjing 210093, China

李政道 教授, 院士

Prof. Academician T. D. Lee  
Department of Physics, Columbia University, New York, NY 10027, USA

李荫远 研究员, 院士  
中国科学院物理研究所, 北京 100190

Prof. Academician Li Yin-Yuan  
Institute of Physics, Chinese Academy of Sciences, Beijing 100190, China

丁肇中 教授, 院士

Prof. Academician Samuel C. C. Ting  
LEP3, CERN, CH-1211, Geneva 23, Switzerland

杨振宁 教授, 院士

Prof. Academician C. N. Yang  
Institute for Theoretical Physics, State University of New York, USA

杨福家 教授, 院士  
复旦大学物理二系, 上海 200433

Prof. Academician Yang Fu-Jia  
Department of Nuclear Physics, Fudan University, Shanghai 200433, China

周光召 研究员, 院士  
中国科学技术协会, 北京 100863

Prof. Academician Zhou Guang-Zhao (Chou Kuang-Chao)  
China Association for Science and Technology, Beijing 100863, China

王乃彦 研究员, 院士  
中国原子能科学研究院, 北京 102413

Prof. Academician Wang Nai-Yan  
China Institute of Atomic Energy, Beijing 102413, China

梁敬魁 研究员, 院士  
中国科学院物理研究所, 北京 100190

Prof. Academician Liang Jing-Kui  
Institute of Physics, Chinese Academy of Sciences, Beijing 100190, China

### 2012-2015

#### 主 编 Editor-in-Chief

欧阳钟灿 研究员, 院士  
中国科学院理论物理研究所,  
北京 100190

Prof. Academician Ouyang Zhong-Can  
Institute of Theoretical Physics, Chinese Academy of Sciences,  
Beijing 100190, China

#### 副主编 Associate Editors

赵忠贤 研究员, 院士  
中国科学院物理研究所, 北京 100190

Prof. Academician Zhao Zhong-Xian  
Institute of Physics, Chinese Academy of Sciences, Beijing 100190, China

杨国桢 研究员, 院士  
中国科学院物理研究所, 北京 100190

Prof. Academician Yang Guo-Zhen  
Institute of Physics, Chinese Academy of Sciences, Beijing 100190, China

张 杰 研究员, 院士  
上海交通大学物理与天文系,  
上海 200240

Prof. Academician Zhang Jie  
Department of Physics and Astronomy, Shanghai Jiao Tong University,  
Shanghai 200240, China

邢定钰 教授, 院士  
南京大学物理学院, 南京 210093  
沈保根 研究员, 院士  
中国科学院物理研究所, 北京 100190  
龚旗煌 教授, 院士  
北京大学物理学院, 北京 100871  
沈平 教授  
香港科技大学物理系, 香港九龍

### 编辑委员 Editorial Board

2011–2016

Prof. F. R. de Boer

Prof. H. F. Braun

陈东敏 教授

冯世平

教授  
北京师范大学物理系, 北京 100875

高鸿钧

研究员, 院士  
中国科学院物理研究所, 北京 100190

顾长志

研究员  
中国科学院物理研究所, 北京 100190

胡岗

教授  
北京师范大学物理系, 北京 100875

侯建国

教授, 院士  
中国科学技术大学中国科学院结构分析  
重点实验室, 合肥 230026

李方华

研究员, 院士  
中国科学院物理研究所, 北京 100190

闵乃本

教授, 院士  
南京大学物理系, 南京 210093

聂玉昕

研究员  
中国科学院物理研究所, 北京 100190

潘建伟

教授, 院士  
中国科学技术大学近代物理系,  
合肥 230026

沈志勋

教授

苏肇冰

研究员, 院士  
中国科学院理论物理研究所,  
北京 100190

孙昌璞

研究员, 院士  
中国科学院理论物理研究所,  
北京 100190

王思哥

研究员, 院士  
北京大学物理学院, 北京 100871

夏建白

研究员, 院士  
中国科学院半导体研究所,  
北京 100083

洗鼎昌

研究员, 院士  
中国科学院高能物理研究所,  
北京 100049

向涛

研究员, 院士  
中国科学院理论物理研究所,  
北京 100190

谢心澄

教授  
北京大学物理学院, 北京 100871

詹文龙

研究员, 院士  
中国科学院, 北京 100864

朱邦芬

教授, 院士  
清华大学物理系, 北京 100084

2013–2018

Prof. Antonio H. Castro Neto

Prof. Chia-Ling Chien

Prof. David Andelman

Prof. Masao Doi

Prof. Michiyoshi Tanaka

Prof. Werner A. Hofer

丁军 教授

贺贤士

研究员, 院士  
北京应用物理与计算数学研究所,  
北京 100088

金晓峰

教授  
复旦大学物理系, 上海 200433

Prof. Academician Xing Ding-Yu  
School of Physics, Nanjing University, Nanjing 210093, China

Prof. Academician Shen Bao-Gen  
Institute of Physics, Chinese Academy of Sciences, Beijing 100190, China

Prof. Academician Gong Qi-Huang  
School of Physics, Peking University, Beijing 100871, China

Prof. Sheng Ping  
Department of Physics, The Hong Kong University of Science and Technology,  
Kowloon, Hong Kong, China

van der Waals-Zeeman Institute der Universiteit van Amsterdam  
Valckenierstraat 65, 1018 XE Amsterdam, **The Netherlands**  
Physikalisches Institut, Universität Bayreuth, D-95440 Bayreuth, **Germany**

Prof. Dong-Min  
Rowland Institute for Science, Harvard University, **USA**

Prof. Feng Shi-Ping  
Department of Physics, Beijing Normal University, Beijing 100875, China

Prof. Academician Gao Hong-Jun  
Institute of Physics, Chinese Academy of Sciences, Beijing 100190, China

Prof. Gu Chang-Zhi  
Institute of Physics, Chinese Academy of Sciences, Beijing 100190, China

Prof. Hu Gang  
Department of Physics, Beijing Normal University, Beijing 100875, China

Prof. Academician Hou Jian-Guo  
Structure Research Laboratory, University of Science and Technology of  
China, Hefei 230026, China

Prof. Academician Li Fang-Hua  
Institute of Physics, Chinese Academy of Sciences, Beijing 100190, China

Prof. Academician Min Nai-Ben  
Department of Physics, Nanjing University, Nanjing 210093, China

Prof. Nie Yu-Xin  
Institute of Physics, Chinese Academy of Sciences, Beijing 100190, China

Prof. Academician Pan Jian-Wei  
Department of Modern Physics, University of Science and Technology of  
China, Hefei 230026, China

Prof. Shen Zhi-Xun  
Stanford University, Stanford, CA 94305-4045, **USA**

Prof. Academician Su Zhao-Bing  
Institute of Theoretical Physics, Chinese Academy of Sciences,  
Beijing 100190, China

Prof. Academician Sun Chang-Pu  
Institute of Theoretical Physics, Chinese Academy of Sciences, Beijing  
100190, China

Prof. Academician Wang En-Ge  
School of Physics, Peking University, Beijing 100871, China

Prof. Academician Xia Jian-Bai  
Institute of Semiconductors, Chinese Academy of Sciences,  
Beijing 100083, China

Prof. Academician Xian Ding-Chang  
Institute of High Energy Physics, Chinese Academy of Sciences,  
Beijing 100049, China

Prof. Academician Xiang Tao  
Institute of Theoretical Physics, Chinese Academy of Sciences,  
Beijing 100190, China

Prof. Xie Xin-Cheng  
School of Physics, Peking University, Beijing 100871, China

Prof. Academician Zhan Wen-Long  
Chinese Academy of Sciences, Beijing 100864, China

Prof. Academician Zhu Bang-Fen  
Department of Physics, Tsinghua University, Beijing 100084, China

Physics Department, Faculty of Science, National University of Singapore,  
Singapore 117546, **Singapore**

Department of Physics and Astronomy, The Johns Hopkins University,  
Baltimore, MD 21218, **USA**

School of Physics and Astronomy, Tel Aviv University, Tel Aviv 69978, **Israel**

Toyota Physical and Chemical Research Institute, Yokomichi, Nagakute,  
Aichi 480-1192, **Japan**

Research Institute for Scientific Measurements, Tohoku University, Katahira  
2-1-1, Aoba-ku 980, Sendai, **Japan**

Stephenson Institute for Renewable Energy, The University of Liverpool,  
Liverpool L69 3BX, **UK**

Prof. Ding Jun  
Department of Materials Science & Engineering, National University of  
Singapore, Singapore 117576, **Singapore**

Prof. Academician He Xian-Tu  
Institute of Applied Physics and Computational Mathematics, Beijing 100088,  
China

Prof. Jin Xiao-Feng  
Department of Physics, Fudan University, Shanghai 200433, China

李儒新 研究员  
中国科学院上海光学精密机械研究所,  
上海 201800

吕力 研究员  
中国科学院物理研究所, 北京 100190

李晓光 教授  
中国科学技术大学物理系, 合肥 230026

沈元壤 教授

王亚愚 教授  
清华大学物理系, 北京 100084

王玉鹏 研究员  
中国科学院物理研究所, 北京 100190

王肇中 教授

闻海虎 教授  
南京大学物理学院系, 南京 210093

徐至展 研究员, 院士  
中国科学院上海光学精密机械研究所,  
上海 201800

许岑珂 助理教授

薛其坤 教授, 院士  
清华大学物理系, 北京 100084

叶军 教授

张振宇 教授

## 2015–2020

Prof. J. Y. Rhee  
Prof. Robert J. Joynt

程建春 教授  
南京大学物理学院, 南京 210093

戴希 研究员  
中国科学院物理研究所, 北京 100190

郭光灿 教授, 院士  
中国科学技术大学物理学院, 合  
肥 230026

刘朝星 助理教授

刘荧 教授  
上海交通大学物理与天文系, 上  
海 200240

龙桂鲁 教授  
清华大学物理系, 北京 100084

牛谦 教授

欧阳颀 教授, 院士  
北京大学物理学院, 北京 100871

孙秀冬 教授  
哈尔滨工业大学物理系, 哈尔滨 150001

童利民 教授  
浙江大学光电信息工程学系, 杭  
州 310027

童彭尔 教授  
香港科技大学物理系, 香港九龍

王开友 研究员  
中国科学院半导体研究所, 北京 100083

魏苏淮 教授

解思深 研究员, 院士  
中国科学院物理研究所, 北京 100190

叶朝辉 研究员, 院士  
中国科学院武汉物理与数学研究所,  
武汉 430071

郁明阳 教授

张富春 教授  
香港大学物理系, 香港

张勇 教授

郑波 教授  
浙江大学物理系, 杭州 310027

周兴江 研究员  
中国科学院物理研究所, 北京 100190

## 编辑 Editorial Staff

王久丽 Wang Jiu-Li 章志英 Zhang Zhi-Ying 蔡建伟 Cai Jian-Wei 翟振 Zhai Zhen 郭红丽 Guo Hong-Li

Prof. Li Ru-Xin  
Shanghai Institute of Optics and Fine Mechanics, Chinese Academy of  
Sciences, Shanghai 201800, China

Prof. Lü Li  
Institute of Physics, Chinese Academy of Sciences, Beijing 100190, China

Prof. Li Xiao-Guang  
Department of Physics, University of Science and Technology of China,  
Hefei 230026, China

Prof. Shen Yuan-Rang  
Lawrence Berkeley National Laboratory, Berkeley, CA 94720, **USA**

Prof. Wang Ya-Yu  
Department of Physics, Tsinghua University, Beijing 100084, China

Prof. Wang Yu-Peng  
Institute of Physics, Chinese Academy of Sciences, Beijing 100190, China

Prof. Wang Zhao-Zhong  
Laboratory for Photonics and Nanostructures(LPN) CNRS-UPR20,  
Route de Nozay, 91460 Marcoussis, **France**

Prof. Wen Hai-Hu  
School of Physics, Nanjing University, Nanjing 210093, China

Prof. Academician Xu Zhi-Zhan  
Shanghai Institute of Optics and Fine Mechanics, Chinese Academy of  
Sciences, Shanghai 201800, China

Assist. Prof. Xu Cen-Ke  
Department of Physics, University of California, Santa Barbara, CA 93106,  
**USA**

Prof. Academician Xue Qi-Kun  
Department of Physics, Tsinghua University, Beijing 100084, China

Prof. Ye Jun  
Department of Physics, University of Colorado, Boulder,  
Colorado 80309-0440, **USA**

Prof. Z. Y. Zhang  
Oak Ridge National Laboratory, Oak Ridge, TN 37831–6032, **USA**

Department of Physics, Sungkyunkwan University, Suwon, **Korea**

Physics Department, University of Wisconsin-Madison, Madison, **USA**

Prof. Cheng Jian-Chun  
School of Physics, Nanjing University, Nanjing 210093, China

Prof. Dai Xi  
Institute of Physics, Chinese Academy of Sciences, Beijing 100190, China

Prof. Academician Guo Guang-Can  
School of Physical Sciences, University of Science and Technology of China,  
Hefei 230026, China

Assist. Prof. Liu Chao-Xing  
Department of Physics, Pennsylvania State University PA 16802-6300, **USA**

Prof. Liu Ying  
Department of Physics and Astronomy, Shanghai Jiao Tong University,  
Shanghai 200240, China

Prof. Long Gui-Lu  
Department of Physics, Tsinghua University, Beijing 100084 China

Prof. Niu Qian  
Department of Physics, University of Texas, Austin, TX 78712, **USA**

Prof. Academician Ouyang Qi  
School of Physics, Peking University, Beijing 100871, China

Prof. Sun Xiu-Dong  
Department of Physics, Harbin Institute of Technology, Harbin 150001, China

Prof. Tong Li-Min  
Department of Optical Engineering, Zhejiang University,  
Hangzhou 310027, China

Prof. Tong Peng-Er  
Department of Physics, The Hong Kong University of Science and Technology,  
Kowloon, Hong Kong, China

Prof. Wang Kai-You  
Institute of Semiconductors, Chinese Academy of Sciences, Beijing 100083,  
China

Prof. Wei Su-Huai  
National Renewable Energy Laboratory, Golden, Colorado 80401-3393, **USA**

Prof. Academician Xie Si-Shen  
Institute of Physics, Chinese Academy of Sciences, Beijing 100190, China

Prof. Academician Ye Chao-Hui  
Wuhan Institute of Physics and Mathematics, Chinese Academy of Sciences,  
Wuhan 430071, China

Prof. Yu Ming-Yang  
Theoretical Physics I, Ruhr University, D-44780 Bochum, **Germany**

Prof. Zhang Fu-Chun  
Department of Physics, The University of Hong Kong, Hong Kong, China

Prof. Zhang Yong  
Electrical and Computer Engineering Department, The University of North  
Carolina at Charlotte, Charlotte, **USA**

Prof. Zheng Bo  
Physics Department, Zhejiang University, Hangzhou 310027, China

Prof. Zhou Xing-Jiang  
Institute of Physics, Chinese Academy of Sciences, Beijing 100190, China

# Simulation of positron backscattering and implantation profiles using Geant4 code\*

Huang Shi-Juan(黄世娟)<sup>a)b)</sup>, Pan Zi-Wen(潘子文)<sup>a)b)</sup>, Liu Jian-Dang(刘建党)<sup>a)b)</sup>,  
Han Rong-Dian(韩荣典)<sup>a)b)</sup>, and Ye Bang-Jiao(叶邦角)<sup>a)b)†</sup>

<sup>a)</sup>Department of Modern Physics, University of Science and Technology of China, Hefei 230026, China

<sup>b)</sup>State Key Laboratory of Particle Detection and Electronics,  
University of Science and Technology of China, Hefei 230026, China

(Received 17 April 2015; revised manuscript received 7 July 2015; published online 20 August 2015)

For the proper interpretation of the experimental data produced in slow positron beam technique, the positron implantation properties are studied carefully using the latest Geant4 code. The simulated backscattering coefficients, the implantation profiles, and the median implantation depths for mono-energetic positrons with energy range from 1 keV to 50 keV normally incident on different crystals are reported. Compared with the previous experimental results, our simulation backscattering coefficients are in reasonable agreement, and we think that the accuracy may be related to the structures of the host materials in the Geant4 code. Based on the reasonable simulated backscattering coefficients, the adjustable parameters of the implantation profiles which are dependent on materials and implantation energies are obtained. The most important point is that we calculate the positron backscattering coefficients and median implantation depths in amorphous polymers for the first time and our simulations are in fairly good agreement with the previous experimental results.

**Keywords:** positron beam, backscattering coefficient, implantation profile, Geant4

**PACS:** 78.70.-g, 78.70.Bj

**DOI:** 10.1088/1674-1056/24/10/107803

## 1. Introduction

In recent decades, the positron annihilation technique<sup>[1]</sup> has been a powerful tool that has been applied for the characterization of defects of materials due to its nondestruction and high sensitivity at the atomic level. The slow positron beam technique can provide depth-resolved information by implanting mono-energetic positrons of energies in the range from a few hundreds of eV to dozens of keV into the samples. The mean implantation depth increases with the increase of energy. Therefore, it is widely used to investigate inhomogeneously distributed defect concentrations in crystalline materials and to study the properties of thin films, surfaces, and interfaces of layered materials.<sup>[1-4]</sup>

We need a detailed knowledge of the depth distribution of positrons in order to analyze the low-energy positron beam experimental data. Two separate parts must be considered, one is the modeling of the thermalization or implantation of the positrons, which can be slowed down to near-thermal energies after a few picoseconds in a material, and the other one is the modeling of the diffusion and subsequent annihilation of the thermalized positrons.<sup>[2-5]</sup> The depth distribution of the thermalized positrons before diffusion is called the implantation or stopping profile. The depth distribution due to diffusion can be obtained by solving the steady-state diffusion equation using the positron implantation profile as a source term. Software has already been developed for diffusion analyses, the most

widely used is the VEPFIT program.<sup>[6-8]</sup> The VEPFIT program is based on the Makhovian distribution, which is derived from firstly fitting the Monte Carlo results.<sup>[9]</sup>

The Makhovian profile

$$P(z, E) = \frac{mz^{m-1}}{z_0^m} \exp \left[ - \left( \frac{z}{z_0} \right)^m \right],$$

$$z_0 = \frac{\bar{z}}{\Gamma[(1/m) + 1]}, \quad \bar{z} = \frac{A}{\rho} E^n, \quad (1)$$

where  $z$  denotes the distance from the surface of the material in the direction of the incoming beam.  $m$ ,  $A$ , and  $n$  are adjustable parameters to fit the data,  $\rho$  is the density of the host material, and  $\Gamma$  is the gamma function. In general,  $m = 2.0$ ,  $n = 1.6$ ,  $A = 4.0$  ( $\mu\text{g}/\text{cm}^2$ )/keV<sup>1.6</sup> are adopted, though they are believed to be a function of both the atomic number  $Z$  of the material and the incident positron energy  $E$ . To reveal and verify this power law, many experiments and Monte Carlo simulations have been done. Mills and Wilson<sup>[10]</sup> measured the transmission of positrons through thin films for the first time. In the following few years, the Monte Carlo schemes of Valkealahti and Nieminen (VN),<sup>[9,11]</sup> Jensen and Walker (JW),<sup>[12,13]</sup> McKeown *et al.* (BNL),<sup>[14]</sup> Ritley *et al.*<sup>[15]</sup> were developed. The discrepancy among them mainly comes from the difference of the cross section, the mean free path, the energy loss function, the polar scattering angle, and they are suitable over different energy ranges. The calculations based on the PENELOPE,<sup>[16]</sup> POS-SPRITE,<sup>[17]</sup> EGSnrc4.0,<sup>[18]</sup> and

\*Project supported by the National Natural Science Foundation of China (Grant Nos. 11175171 and 11105139).

†Corresponding author. E-mail: [bjye@ustc.edu.cn](mailto:bjye@ustc.edu.cn)

Geant4,<sup>[19]</sup> programs were also done. Baker, Coleman, Mäkinen, *et al.*<sup>[20–24]</sup> measured the backscattering coefficients and implantation profiles of the positrons in elemental metals, and Algers *et al.*<sup>[25]</sup> and Palacio *et al.*<sup>[26]</sup> measured the implantation depths of the positrons in polymers. Almost all of them indicate that the fitting parameters of the backscattering coefficients and the implantation profiles are not fixed constants and are dependent on the materials.

It is necessary to point out that the direct measurement of the implantation profiles is very difficult, so far all of these profiles are indirectly obtained from the fitting data which are derived from the positron lifetime spectroscopy or the Doppler broadening spectroscopy.<sup>[21,22,25,26]</sup> In fact, positrons backscattered from the target into the vacuum may return to the sample, while the positrons implanted into the substrate may diffuse into the overlays. These uncontrolled factors lead to the low statistical accuracy of the measured profiles. In the low energy region, their influence could be larger. Therefore, developing simple theoretical calculations or computer simulations is essential. Geant4<sup>[27]</sup> is a very strong toolkit that is dedicated to accurate and comprehensive simulations of the passage of particles through matter over a wide energy range. The atomic data used in this software are extracted from a set of publicly distributed evaluated data libraries. In the latest version, some favorable improvements have been implemented.<sup>[28]</sup> While the backscattering coefficients can be measured easily and correctly, it is feasible to analyze the implantation profiles based on the fact that the simulated backscattering coefficients are in good agreement with the experimental data.

## 2. Simulation details

The normal incident mono-energetic positrons first slow down to the thermal energy through scattering elastically and inelastically in materials, they then diffuse, and they finally annihilate with random electrons. In this paper, we only focus on the first process; that is, the implantation process.

In the first process, positrons interact with the host material through the following ways: the elastic scattering with the nuclei, the inelastic scattering with the electrons, and radiation at high energy. Corresponding to them, we carefully choose five models to simulate the thermalization process in the latest Geant4 (Release 10.1). G4Goudsmit-SaundersonMscModel<sup>[29,30]</sup> is applicable only for electrons and positrons and is fully based on the same theory as Penelope and EGSnrc, we use it to handle the elastic scattering process. G4PenelopeIonisationModel is used to handle ionization and energy loss, G4PenelopeBremsstrahlungModel, G4SynchrotronRadiationModel, and G4PositronNuclearProcess are also included for high energy. The G4PenelopeXXX models are inherited from the PENELOPE code,<sup>[16]</sup> which is

specially used to simulate the interaction between low energy electrons or positrons and materials, and is valid for energies down to a few hundred eV. The cut value is set to 1 nm and the minimum energy is 20 eV. The path length traveled by the positron between 20 eV and near-thermal energies (a few meV) is insignificant compared to the implantation depths. Otherwise, the second particles' interaction is not considered, because we only need the information of the primary particle.

Our simulations are performed for many elemental metals, semiconductors, and polymers. Figure 1 shows the schematic diagram, taking Al as an example. The thickness of each kind of material is set to the order of centimeter, which is far greater than its corresponding positron implantation depth. The implantation positron energies are varied from 1 keV to 50 keV. There is no gap between the incident positron and the material at the beginning. We select the incident energy, and then the energy loss and position change are determined through the five procedures mentioned above. We record the position of the positron when it is slowed down to near zero energy. For the backscattered positrons, their energies are usually high, so we do not record them. The trajectories of  $10^5$  particles implanting normally to the entrance surface are studied. It must be pointed out that the detailed crystal structure of the host material has not been implemented in Geant4, so the crystal effects such as channeling are not modeled, although they may strongly affect the results for some kinds of crystals, we will discuss this in more detail in the following.

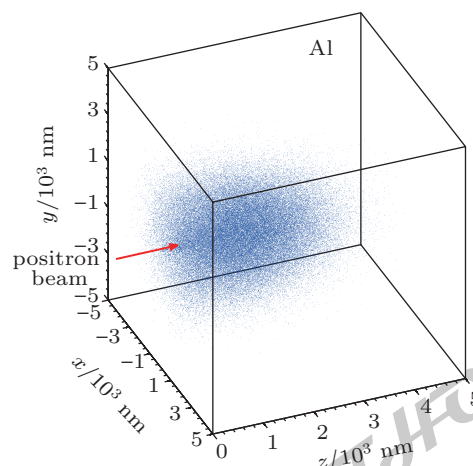


Fig. 1. (color online) The schematic diagram, taking Al as an example. The blue points denote the end positions of the positrons.

## 3. Results and discussion

### 3.1. Backscattering coefficients

The backscattering coefficient is the most accurate quantity for a direct comparison of Monte Carlo simulations of a keV electron and positron slowing down in solids and experimental data. Firstly, we investigate the backscattering coefficients of the elemental crystals including bismuth and actinium

with atomic numbers ranging from 4 to 89 over the energy range 1 keV–50 keV.

### 3.1.1. Al, Cu, Ag, and Au

The backscattering coefficients of Al, Cu, Ag, and Au against implantation positron energy have been widely studied previously. In Fig. 2, we make a comparison of our Monte Carlo results and other simulated and experimental data. The backscattering coefficients increase with the increase of implantation positron energy in the low energy region and they then saturate. Our simulated results for these four crystals are

all in very good agreement with the experimental data reported by Coleman *et al.*<sup>[23]</sup> The experimental data points of Al, Cu, and Ag reported by Baker *et al.*<sup>[20]</sup> are slightly smaller than the others. The Monte Carlo results for Cu reported by Valkealahti and Nieminen<sup>[11]</sup> are clearly bigger than the others when the implantation energy is above 5 keV. The Monte Carlo results of Ag reported by Aydın<sup>[31]</sup> are systematically large compared with our simulations and those of others. There is a great difference between the Monte Carlo results of Au reported by Dryzek and Horodek<sup>[19]</sup> and those of others.

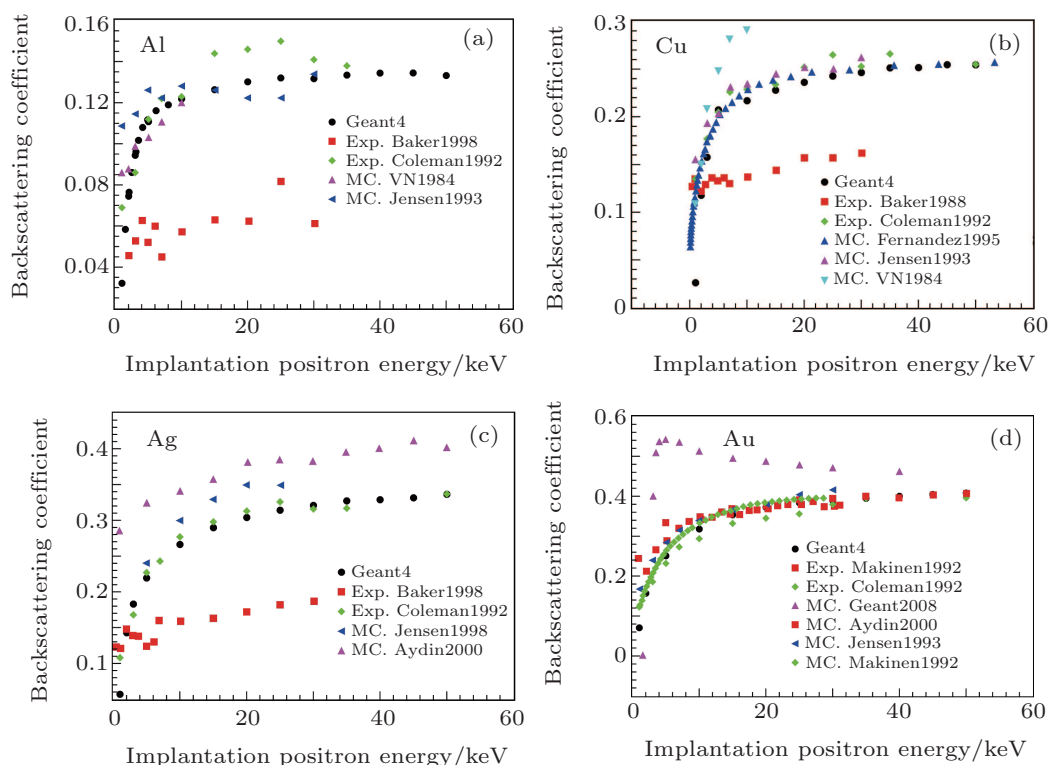


**Fig. 2.** (color online) The backscattering coefficients versus incident positron energy for Al (a); for Cu (b); for Ag (c); for Au (d). Our simulation results (Geant4), Exp. Baker1988 (Ref. [20]), Exp. Coleman1992 (Ref. [23]), MC. VN1984 (Ref. [11]), MC. Jensen1993 (Ref. [13]), MC. Fernandez1995 (Ref. [32]), MC. Aydın2000 (Ref. [31]), MC. Jensen1990 (Ref. [12]), MC. Geant2008 (Ref. [19]), MC. Makinen1992 and Exp. Makinen1992 (Ref. [24]).

### 3.1.2. Be and Zn

In Fig. 3, the backscattering coefficients of Be and Zn versus incident positron energy are presented. Our calculation of Zn seems to be consistent with the experimental data reported by Coleman *et al.*<sup>[23]</sup> For the case of Be, the Monte Carlo results reported by Coleman *et al.*<sup>[23]</sup> and Jensen *et al.*<sup>[13]</sup> are almost identical. According to our best knowledge, there are very few experimental data points of the backscattering coefficients of Be up to now. Although there is only one data point of the backscattering coefficient of Be measured by Massoumi *et al.*<sup>[33]</sup> at 35 keV, it seems to be much closer to our calculations than the other two. For further comparison, more experiments need to be done.

### 3.1.3. C, Si, and Ge

The backscattering coefficients of semiconductors such as graphite, diamond, Si and Ge in diamond structure are presented in Fig. 4. In Geant4, the difference between graphite and diamond is the density, while we obtain almost the same backscattering coefficients for these two crystals, and the experimental data of graphite reported by Makinen *et al.*<sup>[24]</sup> are obviously higher than ours. The results of diamond, Si and Ge reported by Dryzek *et al.*,<sup>[19]</sup> who also used the Geant4 code but selected different models, show that the backscattering coefficient decreases with the increase of implantation energy and saturates at the energies higher than 20 keV, while our results give the opposite trend. This is consistent with the experimental results; however, our results do not fit very well with the experiments and those of others.



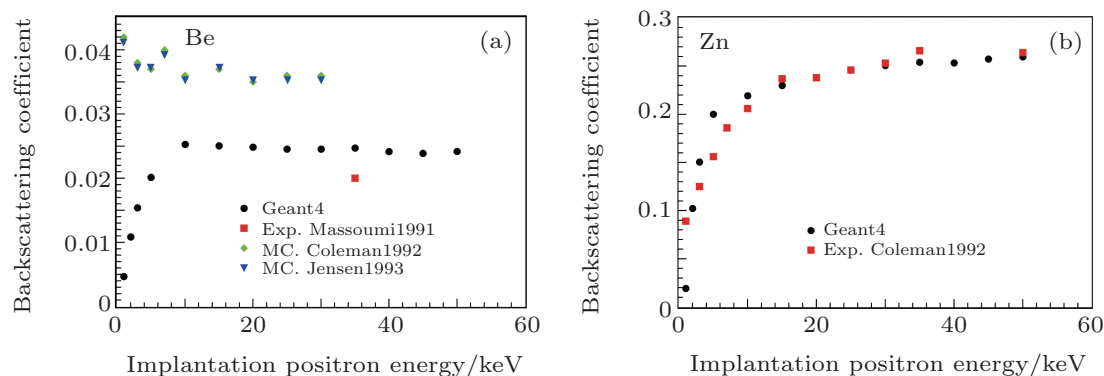


Fig. 3. (color online) The backscattering coefficients versus incident positron energy for Be (a); for Zn (b). Our simulation results (Geant4), Exp. Massoumi1991 (Ref. [33]), MC. Coleman and Exp. Coleman1992 (Ref. [23]), MC. Jensen1993 (Ref. [13]).

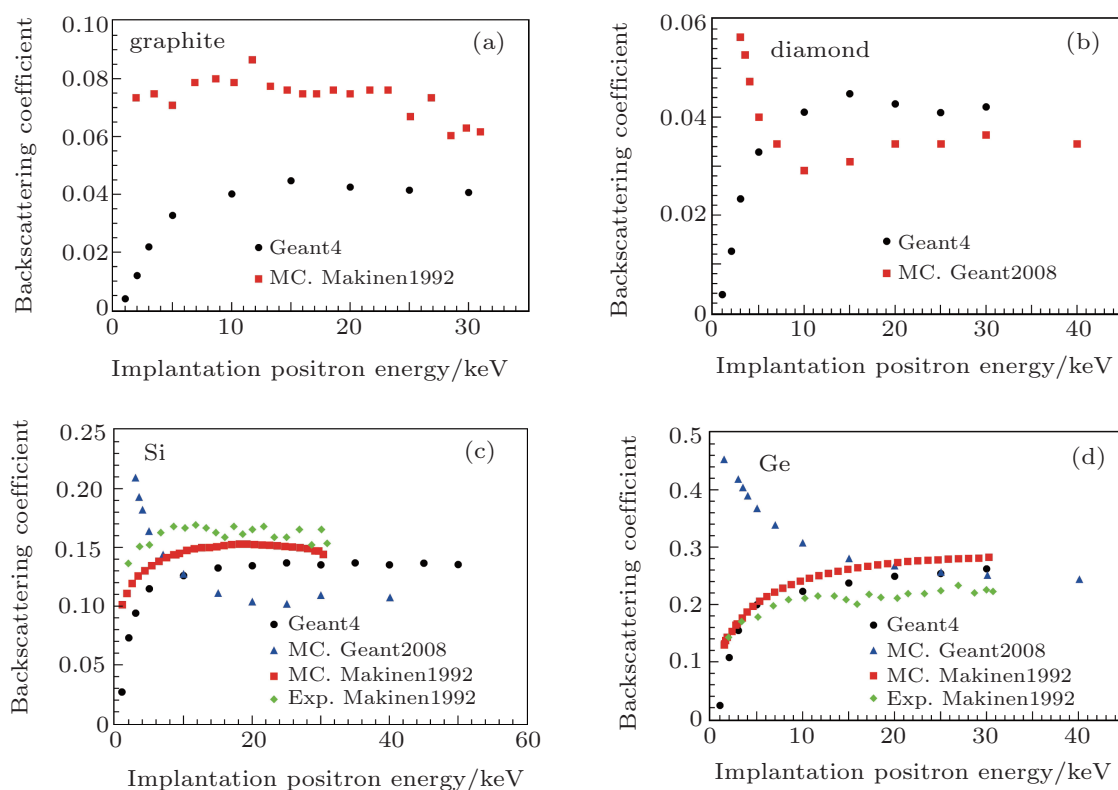


Fig. 4. (color online) The backscattering coefficients versus incident positron energy for graphite (a); for diamond (b); for Si (c); for Ge (d). Our simulation results (Geant4), MC. Makinen1992 and Exp. Makinen1992 (Ref. [24]), MC. Geant2008 (Ref. [19]).

### 3.1.4. W

Because of its low positron affinity, W is widely used as a moderator in the slow positron beam technique. In Fig. 5, we present the relationship between its backscattering coefficients and the incident positron energy. Our results show that the backscattering coefficient increases as the energy increases, while this is very different from the experimental data reported by Baker *et al.*<sup>[20]</sup> which almost saturates at all energies. Although there are only a few data points reported by Makinen *et al.*<sup>[24]</sup> and Coleman *et al.*,<sup>[23]</sup> the trend of their results is similar to ours.

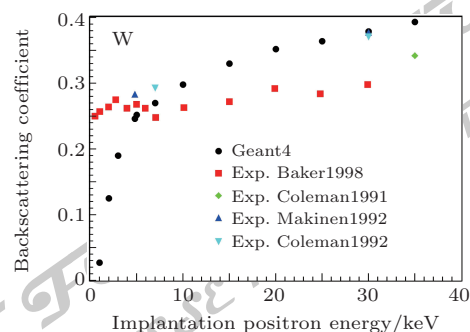


Fig. 5. (color online) The backscattering coefficients versus incident positron energy for W. Our simulation results (Geant4), Exp. Baker1988 (Ref. [20]), Exp. Massoumi1991 (Ref. [33]), Exp. Makinen1992 (Ref. [24]), Exp. Coleman1992 (Ref. [23]).

### 3.1.5. Amorphous polymers

Algers *et al.* [25] and Palacio *et al.* [26] indirectly measured the implantation profiles of the positrons in amorphous polymers, such as atactic polystyrene (PS), atactic poly (methylmethacrylate) (PMMA), and poly (styrene-co-acrylonitrile) (SAN), but there are still no calculations or experimental data of their backscattering coefficients. We calculate these data for the first time and present the relationship between their backscattering coefficients and the incident positron energy in Fig. 6. The backscattering coefficients of these amorphous polymers also increase as the energy increases. However, their values are very low, even less than 5%.

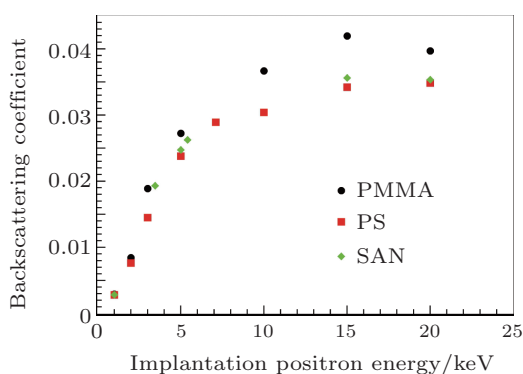


Fig. 6. (color online) The backscattering coefficients versus incident positron energy for amorphous polymers.

### 3.1.6. The backscattering coefficient versus atomic number $Z$

Previous studies have indicated that the backscattering coefficient is not only related to the implantation energy but is also related to the atomic number  $Z$  of the host material. In Fig. 7, we also present our simulations of the backscattering coefficients as a function of atomic number  $Z$  for several values of the positron implantation energy. It can be noticed that the backscattering coefficient increases with the increase of implantation energy and the atomic number, respectively. Moreover, our simulations reproduce the values of the backscattering coefficients and their tendencies fairly well, especially at high energies.

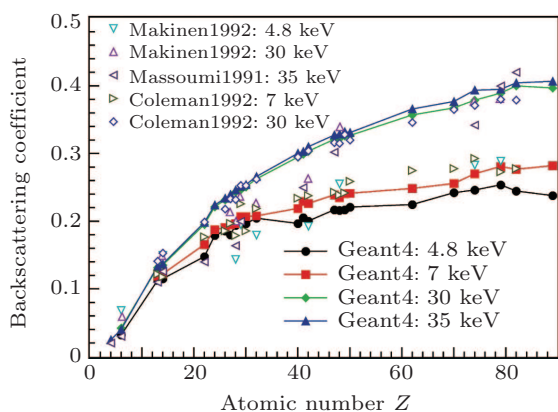


Fig. 7. (color online) The backscattering coefficients as the function of atomic number  $Z$ . Our simulation results (Geant4), Makinen1992 (Ref. [24]), Massoumi1991 (Ref. [33]), Coleman1992 (Ref. [23]).

### 3.1.7. Discussion

From the results listed above, we can notice that there is a big discrepancy among the experimental data measured by different authors, even for the same materials, especially for the low- $Z$  materials and in the low energy region. For low- $Z$  materials, such as Be and graphite, the uncertainties are large because of their small backscattering coefficients. In the low energy region, complications arise from positronium formation at the surface and the sensitivity of low-energy positrons to the surface condition. In addition, the uncertainty of the counts, the possible detection of the annihilation radiation from the backscattered positrons, and the angle of incidence that is not strictly normal to the surface of the target all give rise to the systematic error, and they are very hard to be avoided.

As we know, the elastic scattering process is the main factor to determine the backscattering coefficients in the Monte Carlo program. In our simulations, the backscattering coefficients are in very good agreement with the experimental data and this indicates that our model is reasonable. In Geant4 code, the detailed crystal structure of the host material has not been incorporated; that is to say, the atoms are randomly uniformly distributed and the structure is only up to the density and its atomic number. For crystals with a cubic close packed structure, such as Al, Cu, Ag, and Au and so on, the simulation structures are very close to their actual structures, so the influence of the structure on the backscattering coefficients can be neglected. For Zn with hexagonal close packed structure, similar to Al, Cu, Ag, and Au, our results are very close to the experimental data points. While for the crystals with the diamond structure, our simulations are a little different from the experimental data, so the influence of the structure should be considered carefully. For W with body centered cubic structure, although there are only few experimental data points, we conclude that the influence of the structure may not be neglected and the low positron affinity may be another factor that we should take into account.

### 3.2. Positron implantation profiles

Based on the above discussion, we study the positron implantation profiles in Al, Cu, Zn, Ag, and Au when the implantation positron energies are 10 keV, 20 keV, and 35 keV, respectively. Our simulation profiles of Al are shown in Fig. 8, the shape of the profile becomes wide with the increase of implantation positron energy, the same rule is found for the profiles of Cu, Zn, Ag, and Au, and this is consistent with the previous studies. Otherwise, we make a comparison of our simulation profile and the profile reported by Baker *et al.* [22] of Al at 10 keV, and find that they are in reasonable agreement, except that the peak of our simulation curve is a little higher than theirs. However, it should be mentioned that the red solid line in Fig. 8 denotes a Padé fit of their experimental data, and

the experimental data are higher than the fitting data in fact,<sup>[22]</sup> which means that our simulation results are very close to the experimental data.

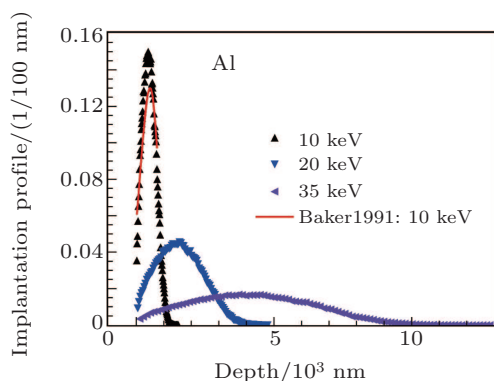


**Fig. 8.** (color online) The positron implantation profiles in Al at 10 keV, 20 keV, and 35 keV. The data of Baker1991 comes from Ref. [22].

We list the parameters from best fits of the Monte Carlo data to Eq. (1) in Table 1. The value of  $m$  decreases with the increase of atomic number  $Z$ , and has a small change versus different implantation energies. For Al, it is very close to the commonly used one, 2.0. In Fig. 9 and Fig. 10, we present the simulation profiles of these five crystals and their corresponding best Makhovian fitting curves when the implantation energies are 10 keV and 35 keV, respectively. It is clear to see that the peak of the fitting curve is more forward and higher than that of our simulation data, especially for the profile of Al at 10 keV, while for the profile of Au at 35 keV, our simulation result is in fairly good agreement with the fitting curve.

**Table 1.** The value of  $m$  from best fits of our Monte Carlo profiles in Al, Cu, Zn, Ag, and Au to Eq. (1) at 10 keV, 20 keV, and 35 keV.

Material	$Z$	Energy/keV	$m$	$\bar{m}$
Al	13	10	1.968	1.975
		20	1.975	
		35	1.983	
Cu	29	10	1.816	1.821
		20	1.817	
		35	1.829	
Zn	30	10	1.817	1.818
		20	1.831	
		35	1.805	
Ag	47	10	1.752	1.755
		20	1.748	
		35	1.766	
Au	70	10	1.725	1.734
		20	1.717	
		35	1.759	

To improve the case mentioned above, Ghosh *et al.*<sup>[14,34]</sup> proposed a modified version of the Makhovian equation, as follows:

$$P(z) = \frac{N_{lm}}{\bar{z}} \left( \frac{z}{c_{lm}\bar{z}} \right)^l \exp \left[ - \left( \frac{z}{c_{lm}\bar{z}} \right)^m \right], \quad (2)$$

where  $N_{lm}$ ,  $l$ ,  $m$ , and  $c_{lm}$  are adjustable parameters. We make a comparison of the best fits to Eq. (1) and Eq. (2) for the profile of Al at 35 keV in Fig. 11. Obviously, our simulation data can also fit well to Eq. (2) with  $N_{lm} = 1.096$ ,  $l = 0.546$ ,  $m = 3.400$ , and  $c_{lm} = 1.589$ . In further study, we find that these parameters are also dependent on the materials and implantation positron energies. Moreover, considerable effort is required if we want to apply it in the VEPFIT program.

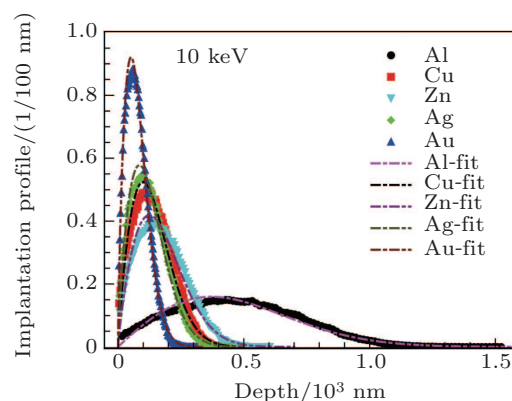


**Fig. 9.** (color online) The simulated positron implantation profiles and their corresponding Makhovian fitting curves in Al, Cu, Zn, Ag, and Au at 10 keV.

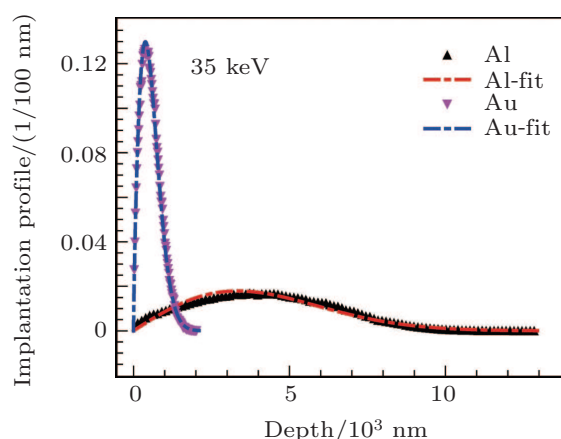


**Fig. 10.** (color online) The simulated positron implantation profiles and their corresponding Makhovian fitting curves in Al and Au at 35 keV.

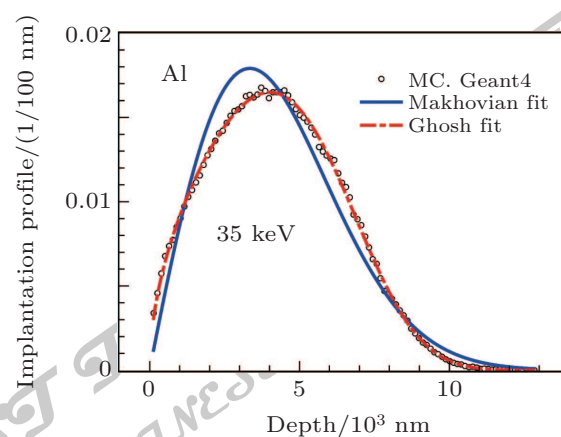


**Fig. 11.** (color online) Our simulated positron implantation profiles in Al at 35 keV and its corresponding Makhovian fitting and Ghosh fitting curves.

### 3.3. Mean implantation depths and median implantation depths

We also investigate the mean implantation depths of the positrons in several metals, in which the positron backscattering coefficients are reproduced well by the latest Geant4 code. We find that all of our simulations can fit well to the equation:  $\bar{z} = (A/\rho)E^n$ , as shown in Fig. 12. The adjustable parameters  $A$  and  $n$  from the best fits of our Monte Carlo data are listed in Table 2. The fitting values of  $A$  are systematically smaller and those of  $n$  are larger than the common used ones.

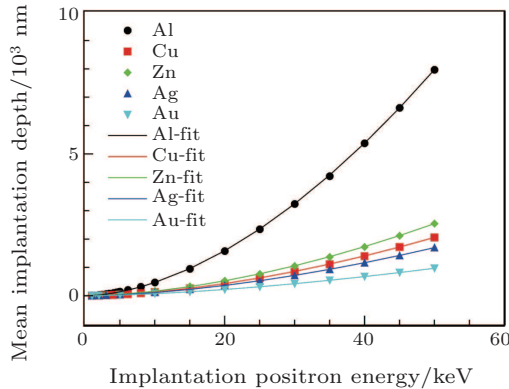


Fig. 12. (color online) The mean depths versus the implantation positron energy for Al, Cu, Zn, Ag, and Au.

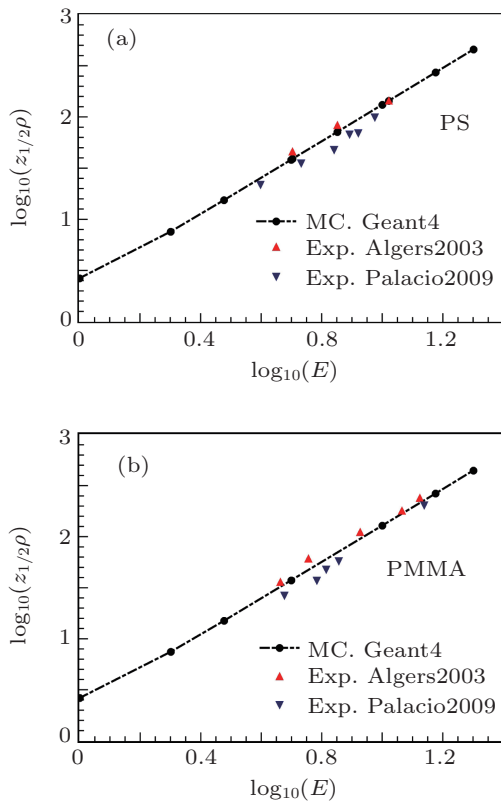


Fig. 13. (color online) Comparison of our simulations and the experimental data for PS (a); for PMMA (b). Our simulation results (Geant4), Exp. Algers2003 (Ref. [25]), Exp. Palacio2009 (Ref. [26]).

Alger *et al.*<sup>[25]</sup> and Palacio *et al.*<sup>[26]</sup> have measured the positron median implantation depths of the positrons in amor-

phous polymers PS and PMMA indirectly. To our best knowledge, there has not yet been theoretical calculation of them. In this paper, we calculate their positron backscattering coefficients and median implantation depths for the first time, at the same time, we compare our calculation results of the median implantation depths with the experimental data reported by Algers *et al.* and Palacio *et al.*, as shown in Fig. 13. Our simulations for either PS or PMMA seem to be much closer to that reported by Algers *et al.* Further, we obtain the values of the fitting parameters  $A_{1/2}$  and  $n$  and list them in Table 2.

Table 2. The values of the fitting parameters  $A$  and  $n$  in the power-law fit of the mean implantation depth  $\bar{z} = (A/\rho)E^n$  for Al, Cu, Zn, Ag, and Au.

Material	Z	Density/(g/cm <sup>3</sup> )	$A/(\mu\text{g}/\text{cm}^2)$	$n$
Al	13	2.70	2.18	1.763 ( $\pm 0.003$ )
Cu	29	8.96	2.27	1.713 ( $\pm 0.006$ )
Zn	30	7.14	2.18	1.719 ( $\pm 0.007$ )
Ag	47	10.5	2.47	1.682 ( $\pm 0.008$ )
Au	79	18.3	3.42	1.612 ( $\pm 0.006$ )
Amorphous polymers				
PS	–	1.040	2.40	1.739 ( $\pm 0.018$ )
PMMA	–	1.197	2.38	1.733 ( $\pm 0.024$ )

According to the discussions above, the positron backscattering coefficients of PS and PMMA are very low, so the influence of the backscattering positrons on experiments should be very weak. The fact that our simulations of amorphous polymers are very close to the experimental data indicates that it is feasible to simulate the implantation profiles using the latest Geant4 code, at least in amorphous polymers.

## 4. Summary

In this paper, we simulated the positron backscattering coefficients, implantation profiles, and mean implantation depths for mono-energetic positrons with an energy range from 1 keV to 50 keV normally incident on metals, semiconductors, and amorphous polymers using the latest Geant4 code. Compared with the previous experimental results, especially in high positron implantation energy region, our simulation backscattering coefficients of Al, Cu, Zn, Ag, and Au with the close packed structure are in fairly good agreement with them, while for the backscattering coefficients of Be, graphite, and diamond with low-Z, Si and Ge with the diamond structure, there exists a discrepancy between our simulations and the experimental data. Considering that the detailed crystal structure of the host material has not been incorporated, we think the accuracy may be related to the structures of the host materials in Geant4.

Based on the reasonable simulated backscattering coefficients, we investigated the implantation profiles and mean depths of Al, Cu, Zn, Ag, Au, PS, and PMMA. The implanta-

tion profiles are well consistent with the Makhovian distribution and the form proposed by Ghosh *et al.*, in some ways, our simulations can fit better than the results in the latter, while the fact that the four adjustable parameters are dependent on materials and implantation energies causes some trouble. The values of  $m$  from the best fits of our simulation data to Eq. (1) decrease with the increase of atomic number  $Z$ , and have a small change versus different implantation energies. For Al, it is very close to 2.0, which is used as the common value. The relationship between the mean implantation depth and the implantation energy well obeys the exponential distribution. The fitting values of  $A$  are systematically smaller and those of  $n$  are larger than the commonly used ones.

We calculated the positron backscattering coefficients and median implantation depths of the positrons in amorphous polymers PS and PMMA for the first time, the backscattering coefficients are very low compared with the other crystals. Our simulated median implantation depths are in fairly good agreement with the previous experimental results. Combined with our discussion above, we think it is simple and feasible to simulate the implantation profiles using the latest Geant4 code, and this has significant consequences for the convenient calculation of positron implantation, especially in elemental and multilayer systems.

## Acknowledgment

We would like to thank Xiao Ran, Liu Yan-Fen and Xu Wen-Zhen for helpful discussions

## References

- [1] Krause-Rehberg R and Leipner H S 1999 *Positron Annihilation in Semiconductors: Defect Studies* (Berlin: Springer-Verlag)
- [2] Schultz Peter J and Lynn K G 1988 *Rev. Mod. Phys.* **60** 701
- [3] Puska M J and Nieminen R M 1994 *Rev. Mod. Phys.* **66** 841
- [4] Tuomisto F and Makkonen I 2013 *Rev. Mod. Phys.* **85** 1583
- [5] Vehanen A, Saarinen K, Hautojärvi P and Huomo H 1987 *Phys. Rev. B* **35** 4606

- [6] Veen A van, Schut H, Vries J de, Hakvoort R A and Ijpma M R 1991 *AIP Conf. Proc.* **218** 171
- [7] Veen A van, Schut H, Clement M, Nijs J M M de, Kruseman A and Ijpma M R 1995 *Appl. Surf. Sci.* **85** 216
- [8] Saleh A S 2013 *J. Theor. Appl. Phys.* **7:39** 1
- [9] Valkealahti S and Nieminen R M 1983 *Appl. Phys. A* **32** 95
- [10] Mills A P and Wilson R J 1982 *Phys. Rev. A* **26** 490
- [11] Valkealahti S and Nieminen R M 1984 *Appl. Phys. A* **35** 51
- [12] Jensen K O, Walker A B and Bouarissa N 1990 *AIP Conf. Proc.* **218** 17
- [13] Jensen K O and Walker A B 1993 *Surf. Sci.* **292** 83
- [14] Ghosh V J, Welch D O and Lynn K G 1993 *Proceedings of the 5th International Workshop on Slow-Positron Beam Techniques for Solids and Surfaces* p. 37
- [15] Ritley K A, Lynn K G, Ghosh V J, Welch D O and McKeown M 1993 *J. Appl. Phys.* **74** 3479
- [16] Baró J, Sempau J, Fernández-Vareac J M and Salvat F 1995 *Nucl. Instrum. Method Phys. Res. B* **100** 31
- [17] Ritley K A, Ghosh V J, Lynn K G, McKeown M and Welch D O 1998 *Comput. Phys. Commun.* **109** 93
- [18] Treurniet J R and Rogers D W O 1999 *NRC Report PIRS 0669*
- [19] Jerzy Dryzek and Pawel Horodek 2008 *Nucl. Instrum. Method Phys. Res. B* **266** 4000
- [20] Baker J A and Coleman P G 1988 *J. Phys. C: Solid State Phys.* **21** L875
- [21] Baker J A, Chilton N B, Jensen K O, Walker A B and Coleman P G 1991 *Appl. Phys. Lett.* **59** 2962
- [22] Baker J A, Chilton N B, Jensen K O, Walker A B and Coleman P G 1991 *J. Phys.: Condens. Matter* **3** 4109
- [23] Coleman P G, Albrecht L, Jensen K O and Walker A B 1992 *J. Phys.: Condens. Matter* **4** 10311
- [24] Makinen J, Palko S, Martikainen J and Hautojärvi P 1992 *J. Phys.: Condens. Matter* **4** L503
- [25] Algers J, Sperr P, Egger W, Kögel G and Maurer F H J 2003 *Phys. Rev. B* **67** 125404
- [26] Palacio Carlos A, Baerdemaeker Jérémie De, Segers Danny, Mostafa Khaled M, Thourhout Dries Van and Dauwe Charles 2009 *Mater. Sci. Forum* **607** 105
- [27] Agostinelli S, Allison J, Amako K, *et al.* 2003 *Nucl. Instrum. Method Phys. Res. A* **506** 250
- [28] Geant4 web page: <http://www.geant4.org/geant4/>
- [29] Goudsmit S and Saunderson J L 1940 *Phys. Rev.* **57** 24
- [30] Ivanchenko V N, Kadri O, Maire M and Urban L 2010 *J. Phys.: Conf. Ser.* **219** 032045
- [31] Aydın Asuman 2000 *Radiat. Phys. Chem.* **59** 277
- [32] Fernández-Varea J M, Liljequist D, Csillag S, Rätty R and Salvat F 1996 *Nucl. Instrum. Method Phys. Res. B* **108** 35
- [33] Massoumi G R, Hozhabri N, Lennard W N and Schultz P J 1991 *Phys. Rev. B* **44** 3486
- [34] Ghosh V J and Aers G C 1995 *Phys. Rev. B* **51** 45

JUST FOR AUTHORS  
 — CHINESE PHYSICS B

# Chinese Physics B

Volume 24

Number 10

October 2015

## GENERAL

- 100101 Rapid identifying high-influence nodes in complex networks**  
Song Bo, Jiang Guo-Ping, Song Yu-Rong and Xia Ling-Ling
- 100201 Singular and non-topological soliton solutions for nonlinear fractional differential equations**  
Ozkan Guner
- 100202 Analysis of elastoplasticity problems using an improved complex variable element-free Galerkin method**  
Cheng Yu-Min, Liu Chao, Bai Fu-Nong and Peng Miao-Juan
- 100203 Conservative method for simulation of a high-order nonlinear Schrödinger equation with a trapped term**  
Cai Jia-Xiang, Bai Chuan-Zhi and Qin Zhi-Lin
- 100204 Transformation optics for efficient calculation of transmembrane voltage induced on cells**  
Liao Yin-Hong, Zhu Hua-Cheng, Tang Zheng-Ming and Huang Ka-Ma
- 100301 Time-domain nature of group delay**  
Wang Jian-Wu and Feng Zheng-He
- 100302 A new kind of special function and its application**  
Fan Hong-Yi, Wan Zhi-Long, Wu Ze and Zhang Peng-Fei
- 100303 Shannon information entropies for position-dependent mass Schrödinger problem with a hyperbolic well**  
Sun Guo-Hua, Dušan Popov, Oscar Camacho-Nieto and Dong Shi-Hai
- 100304 Characterizing the dynamics of quantum discord under phase damping with POVM measurements**  
Jiang Feng-Jian, Ye Jian-Feng, Yan Xin-Hu and Lü Hai-Jiang
- 100305 Non-Markovianity of a qubit coupled with an isotropic Lipkin–Meshkov–Glick bath**  
Tian Li-Jun, Ti Min-Min and Zhai Xiang-Dong
- 100306 Scheme for purifying a general mixed entangled state and its linear optical implementation**  
Dong Dong, Zhang Yan-Lei, Zou Chang-Ling, Zou Xu-Bo and Guo Guang-Can
- 100307 Deterministic joint remote state preparation of arbitrary single- and two-qubit states**  
Chen Na, Quan Dong-Xiao, Xu Fu-Fang, Yang Hong and Pei Chang-Xing
- 100501 A perturbation method to the tent map based on Lyapunov exponent and its application**  
Cao Lv-Chen, Luo Yu-Ling, Qiu Sen-Hui and Liu Jun-Xiu
- 100502 A novel adaptive-impulsive synchronization of fractional-order chaotic systems**  
Leung Y. T. Andrew, Li Xian-Feng, Chu Yan-Dong and Zhang Hui
- 100503 Synchronization of coupled chaotic Hindmarsh Rose neurons: An adaptive approach**  
Wei Wei
- 100504 Dynamics and stabilization of peak current-mode controlled buck converter with constant current load**  
Leng Min-Rui, Zhou Guo-Hua, Zhang Kai-Tun and Li Zhen-Hua

*(Continued on the Bookbinding Inside Back Cover)*

## ATOMIC AND MOLECULAR PHYSICS

- 103201 The ac Stark shifts of the terahertz clock transitions of barium**  
Yu Geng-Hua, Geng Ying-Ge, Li Long, Zhou Chao, Duan Cheng-Bo, Chai Rui-Peng and Yang Yong-Ming
- 103202 Extreme ultraviolet and x-ray transition wavelengths in Rb XXIV**  
Indu Khatri, Arun Goyal, Sunny Aggarwal, A. K. Singh and Man Mohan
- 103203 Role of elastic scattering in high-order above threshold ionization**  
Chen Zhang-Jin, Ye Jian-Mian and Xu Yang-Bing
- 103204 The VMI study on angular distribution of ejected electrons from Eu  $4f^7 6p_{1/2} 6d$  autoionizing states**  
Zhang Kai, Shen Li, Dong Cheng and Dai Chang-Jian
- 103401 Resonant charge transfer in slow  $\text{Li}^+ - \text{Li}(2s)$  collisions**  
Li Tie-Cheng, Liu Chun-Hua, Qu Yi-Zhi, Liu Ling, Wu Yong, Wang Jian-Guo, Liebermann H. P. and Buenker R. J.
- 103402 Site preferences and lattice vibrations of  $\text{Nd}_6\text{Fe}_{13-x}\text{T}_x\text{Si}$  ( $T = \text{Co}, \text{Ni}$ )**  
Huang Tian-Shun, Cheng Hai-Xia, Wang Xiao-Xu, Zhang Zhen-Feng, An Zhi-Wei and Zhang Guo-Hua
- 103403 Single ionization of helium atoms by energetic fully stripped carbon ions**  
Ebrahim Ghanbari-Adivi and Sadjad Eskandari
- 103601 Modeling the interaction of nitrate anions with ozone and atmospheric moisture**  
A. Y. Galashev

## ELECTROMAGNETISM, OPTICS, ACOUSTICS, HEAT TRANSFER, CLASSICAL MECHANICS, AND FLUID DYNAMICS

- 104101 Reciprocity principle-based model for shielding effectiveness prediction of a rectangular cavity with a covered aperture**  
Jiao Chong-Qing and Li Yue-Yue
- 104102 Design and development of high linearity millimeter wave traveling-wave tube for satellite communications**  
He Jun, Huang Ming-Guang, Li Xian-Xia, Li Hai-Qiang, Zhao Lei, Zhao Jian-Dong, Li Yue and Zhao Shi-Lei
- 104103 Exploring electromagnetic response of tellurium dielectric resonator metamaterial at the infrared wavelengths**  
Song Jia-Kun, Song Yu-Zhi, Li Kang-Wen, Zhang Zu-Yin, Xu Yun, Wei Xin and Song Guo-Feng
- 104104 Tunable wideband absorber based on resistively loaded lossy high-impedance surface**  
Dang Ke-Zheng, Shi Jia-Ming, Wang Jia-Chun, Lin Zhi-Dan and Wang Qi-Chao
- 104201 Absorption enhancement in thin film a-Si solar cells with double-sided  $\text{SiO}_2$  particle layers**  
Chen Le, Wang Qing-Kang, Shen Xiang-Qian, Chen Wen, Huang Kun and Liu Dai-Ming
- 104202 Superscattering-enhanced narrow band forward scattering antenna**  
Hu De-Jiao, Zhang Zhi-You and Du Jing-Lei
- 104203 Ghost imaging with broad distance**  
Duan De-Yang, Zhang Lu, Du Shao-Jiang and Xia Yun-Jie

*(Continued on the Bookbinding Inside Back Cover)*

- 104204 An iterative virtual projection method to improve the reconstruction performance for ill-posed emission tomographic problems**  
Liu Hua-Wei, Zheng Shu and Zhou Huai-Chun
- 104205 Field-free orientation of diatomic molecule via the linearly polarized resonant pulses**  
Li Su-Yu, Guo Fu-Ming, Wang Jun, Yang Yu-Jun and Jin Ming-Xing
- 104206 Photon pair source via two coupling single quantum emitters**  
Peng Yong-Gang and Zheng Yu-Jun
- 104207 Movement of a millimeter-sized oil drop pushed by optical force**  
Zhang Li and She Wei-Long
- 104208 Entanglements in a coupled cavity–array with one oscillating end-mirror**  
Wu Qin, Xiao Yin and Zhang Zhi-Ming
- 104209 Plasmonic emission and plasma lattice structures induced by pulsed laser in Purcell cavity on silicon**  
Huang Wei-Qi, Huang Zhong-Mei, Miao Xin-Jian, Liu Shi-Rong and Qin Chao-Jian
- 104210 Analysis of gain distribution in cladding-pumped thulium-doped fiber laser and optical feedback inhibition problem in fiber-bulk laser system**  
Ji En-Cai, Liu Qiang, Hu Zhen-Yue and Gong Ma-Li
- 104211 Arbitrary frequency stabilization of a diode laser based on visual Labview PID VI and sound card output**  
Feng Guo-Sheng, Wu Ji-Zhou, Wang Xiao-Feng, Zheng Ning-Xuan, Li Yu-Qing, Ma Jie, Xiao Lian-Tuan and Jia Suo-Tang
- 104212 Broadband and high-speed swept external-cavity laser using a quantum-dot superluminescent diode as gain device**  
Hu Fa-Jie, Jin Peng, Wu Yan-Hua, Wang Fei-Fei, Wei Heng and Wang Zhan-Guo
- 104213 An optical fiber spool for laser stabilization with reduced acceleration sensitivity to  $10^{-12}/g$**   
Hu Yong-Qi, Dong Jing, Huang Jun-Chao, Li Tang and Liu Liang
- 104214 V–L decomposition of a novel full-waveform lidar system based on virtual instrument technique**  
Xu Fan and Wang Yuan-Qing
- 104215 Confinement-induced nanocrystal alignment of conjugated polymer by the soft-stamped nanoimprint lithography**  
Li Xiao-Hui, Yu Ji-Cheng, Lu Nai-Yan, Zhang Wei-Dong, Weng Yu-Yan and Gu Zhen
- 104216 Analysis of the spatial filter of a dielectric multilayer film reflective cutoff filter-combination device**  
Zhang Ying, Qi Hong-Ji, Yi Kui, Wang Yan-Zhi, Sui Zhan and Shao Jian-Da
- 104301 Quantitative calculation of reaction performance in sonochemical reactor by bubble dynamics**  
Xu Zheng, Yasuda Keiji and Liu Xiao-Jun
- 104302 Wavefront modulation of water surface wave by a metasurface**  
Sun Hai-Tao, Cheng Ying, Wang Jing-Shi and Liu Xiao-Jun



**104303 Temperature imaging with speed of ultrasonic transmission tomography for medical treatment control: A physical model-based method**

Chu Zhe-Qi, Yuan Jie, Stephen Z. Pinter, Oliver D. Kripfgans, Wang Xue-Ding, Paul L. Carson and Liu Xiao-Jun

**104501 Nonlinear parametrically excited vibration and active control of gear pair system with time-varying characteristic**

Liu Shuang, Wang Jin-Jin, Liu Jin-Jie and Li Ya-Qian

**104502 Skew-gradient representation of generalized Birkhoffian system**

Mei Feng-Xiang and Wu Hui-Bin

**104701 Effects of the computational domain on the secondary flow in turbulent plane Couette flow**

Gai Jie, Xia Zhen-Hua and Cai Qing-Dong

**104702 Ferrofluid nucleus phase transitions in an external uniform magnetic field**

B. M. Tanygin, S. I. Shulyma, V. F. Kovalenko and M. V. Petrychuk

**PHYSICS OF GASES, PLASMAS, AND ELECTRIC DISCHARGES**

**105101 Dynamic mechanical analysis of single walled carbon nanotubes/polymethyl methacrylate nanocomposite films**

Ali Badawi and N. Al-Hosiny

**105102 Effect of microwave frequency on plasma formation in air breakdown at atmospheric pressure**

Zhao Peng-Cheng, Guo Li-Xin and Li Hui-Min

**105201 Investigation of high sensitivity radio-frequency readout circuit based on AlGaIn/GaN high electron mobility transistor**

Zhang Xiao-Yu, Tan Ren-Bing, Sun Jian-Dong, Li Xin-Xing, Zhou Yu, Lü Li and Qin Hua

**CONDENSED MATTER: STRUCTURAL, MECHANICAL, AND THERMAL PROPERTIES**

**106101 Complementary method to locate atomic coordinates by combined searching method of structure-sensitive indexes based on bond valence method**

Song Zhen, Liu Xiao-Lang, He Li-Zhu, Xia Zhi-Guo and Liu Quan-Lin

**106102 Influences of surface and flexoelectric polarization on the effective anchoring energy in nematic liquid crystal**

Guan Rong-Hua, Ye Wen-Jiang and Xing Hong-Yu

**106103 Determination of electrostatic parameters of a coumarin derivative compound  $C_{17}H_{13}NO_3$  by x-ray and density functional theory**

Youcef Megrouss, Nadia Benhalima, Rawia Bahoussi, Nouredine Boukabcha, Abdelkader Chouaih and Fodil Hamzaoui

**106104 New crystal structure and physical properties of TcB from first-principles calculations**

Zhang Gang-Tai, Bai Ting-Ting, Yan Hai-Yan and Zhao Ya-Ru

**106105 Influences of neutral oxygen vacancies and  $E'_1$  centers on  $\alpha$ -quartz**

Li Hui-Ran, Cheng Xin-Lu, Zhang Hong and Zhao Feng

**106106 Analysis of functional failure mode of commercial deep sub-micron SRAM induced by total dose irradiation**

Zheng Qi-Wen, Cui Jiang-Wei, Zhou Hang, Yu De-Zhao, Yu Xue-Feng, Lu Wu, Guo Qi and Ren Di-Yuan

**106601 Analysis of recoverable and permanent components of threshold voltage shift in NBT stressed p-channel power VDMOSFET**

Danijel Danković, Ninoslav Stojadinović, Zoran Prijić, Ivica Manić, Vojkan Davidović, Aneta Prijić, Snežana Djorić-Veljković and Snežana Golubović

**106801 Mechanical strains in pecvd SiN<sub>x</sub>:H films for nanophotonic application**

O. Semenova, A. Kozelskaya, Li Zhi-Yong, and Yu Yu-De

**CONDENSED MATTER: ELECTRONIC STRUCTURE, ELECTRICAL, MAGNETIC, AND OPTICAL PROPERTIES**

**107101 Structural, elastic, and electronic properties of sodium atoms encapsulated type-I silicon-clathrate compound under high pressure**

Zhang Wei, Chen Qing-Yun, Zeng Zhao-Yi and Cai Ling-Cang

**107102 Nano LaAlO<sub>3</sub> buffer layer-assisted tunneling current in manganite p-n heterojunction**

Ma Jun-Jie, Wang Deng-Jing, Huang Hai-Lin, Wang Ru-Wu and Li Yun-Bao

**107301 Influences of Pr and Ta doping concentration on the characteristic features of FTO thin film deposited by spray pyrolysis**

Güven Turgut, Adem Koçyiğit and Erdal Sönmez

**107302 High response Schottky ultraviolet photodetector formed by PEDOT:PSS transparent electrode contacts to Mg<sub>0.1</sub>Zn<sub>0.9</sub>O**

Hu Zuo-Fu, Wu Huai-Hao, Lv Yan-Wu and Zhang Xi-Qing

**107303 Effect of the annealing temperature on the long-term thermal stability of Pt/Si/Ta/Ti/4H-SiC contacts**

Cheng Yue, Zhao Gao-Jie, Liu Yi-Hong, Sun Yu-Jun, Wang Tao and Chen Zhi-Zhan

**107304 Rectification and electroluminescence of nanostructured GaN/Si heterojunction based on silicon nanoporous pillar array**

Wang Xiao-Bo, Li Yong, Yan Ling-Ling and Li Xin-Jian

**107305 A C-band 55% PAE high gain two-stage power amplifier based on AlGaIn/GaN HEMT**

Zheng Jia-Xin, Ma Xiao-Hua, Lu Yang, Zhao Bo-Chao, Zhang Hong-He, Zhang Meng, Cao Meng-Yi and Hao Yue

**107306 Fermi level pinning effects at gate-dielectric interfaces influenced by interface state densities**

Hong Wen-Ting, Han Wei-Hua, Lyu Qi-Feng, Wang Hao and Yang Fu-Hua

**107307 Lateral resistance reduction induced by light-controlled leak current in silicon-based Schottky junction**

Wang Shuan-Hu, Zhang Xu, Zou Lv-Kuan, Zhao Jing, Wang Wen-Xin and Sun Ji-Rong

**107501 Magnetic hysteresis, compensation behaviors, and phase diagrams of bilayer honeycomb lattices**

Ersin Kantar

- 107502 Exact solution of Heisenberg model with site-dependent exchange couplings and Dzyloshinsky–Moriya interaction**  
Yang Li-Jun, Cao Jun-Peng and Yang Wen-Li
- 107503 Effects of oxidation of DyH<sub>3</sub> in Nd–Fe–B sintered magnets**  
Yan Gao-Lin and Fang Zhi-Hao
- 107504 Effects of R-site compositions on the meta-magnetic behavior of Tb<sub>1-x</sub>Pr<sub>x</sub>(Fe<sub>0.4</sub>Co<sub>0.6</sub>)<sub>1.88</sub>C<sub>0.05</sub> (x = 0, 0.8, and 1)**  
Huang Jun-Wei, Xia Zheng-Cai, Cheng Gang, Shi Li-Ran, Jin Zhao, Shang Cui and Wei Meng
- 107505 Magnetic–optical bifunctional CoPt<sub>3</sub>/Co multilayered nanowire arrays**  
Su Yi-Kun, Yan Zhi-Long, Wu Xi-Ming, Liu Huan, Ren Xiao and Yang Hai-Tao
- 107506 Lumped-equivalent circuit model for multi-stage cascaded magnetoelectric dual-tunable bandpass filter**  
Zhang Qiu-Shi, Zhu Feng-Jie and Zhou Hao-Miao
- 107701 The interface density dependence of the electrical properties of 0.9Pb(Sc<sub>0.5</sub>Ta<sub>0.5</sub>)O<sub>3</sub>–0.1PbTiO<sub>3</sub>/0.55Pb(Sc<sub>0.5</sub>Ta<sub>0.5</sub>)O<sub>3</sub>–0.45PbTiO<sub>3</sub> multilayer thin films**  
Li Xue-Dong, Liu Hong, Wu Jia-Gang, Liu Gang, Xiao Ding-Quan and Zhu Jian-Guo
- 107702 Nanoscale domain switching mechanism of Bi<sub>3.15</sub>Eu<sub>0.85</sub>Ti<sub>3</sub>O<sub>12</sub> thin film under the different mechanical forces**  
Zhu Zhe, Chen Yu-Bo and Zheng Xue-Jun
- 107703 Effects of surface adsorbed oxygen, applied voltage, and temperature on UV photoresponse of ZnO nanorods**  
Zong Xian-Li and Zhu Rong
- 107704 C–H complex defects and their influence in ZnO single crystal**  
Xie Hui, Zhao You-Wen, Liu Tong, Dong Zhi-Yuan, Yang Jun and Liu Jing-Ming
- 107705 Temperature dependences of ferroelectricity and resistive switching behavior of epitaxial BiFeO<sub>3</sub> thin films**  
Lu Zeng-Xing, Song Xiao, Zhao Li-Na, Li Zhong-Wen, Lin Yuan-Bin, Zeng Min, Zhang Zhang, Lu Xu-Bing, Wu Su-Juan, Gao Xing-Sen, Yan Zhi-Bo and Liu Jun-Ming
- 107801 Multifunctional disk device for optical switch and temperature sensor**  
Bian Zhen-Yu, Liang Rui-Sheng, Zhang Yu-Jing, Yi Li-Xuan, Lai Gen and Zhao Rui-Tong
- 107802 Single-layer dual-band terahertz filter with weak coupling between two neighboring cross slots**  
Qi Li-Mei, Li Chao, Fang Guang-You and Li Shi-Chao
- 107803 Simulation of positron backscattering and implantation profiles using Geant4 code**  
Huang Shi-Juan, Pan Zi-Wen, Liu Jian-Dang, Han Rong-Dian and Ye Bang-Jiao
- 107804 Exploring positron characteristics utilizing two new positron–electron correlation schemes based on multiple electronic structure calculation methods**  
Zhang Wen-Shuai, Gu Bing-Chuan, Han Xiao-Xi, Liu Jian-Dang and Ye Bang-Jiao

*(Continued on the Bookbinding Inside Back Cover)*

INTERDISCIPLINARY PHYSICS AND RELATED AREAS OF SCIENCE AND TECHNOLOGY

- 108101 Temperature-dependent photoluminescence spectra of GaN epitaxial layer grown on Si (111) substrate**  
Zhao Dan-Mei, Zhao De-Gang, Jiang De-Sheng, Liu Zong-Shun, Zhu Jian-Jun, Chen Ping, Liu Wei, Li Xiang and Shi Ming
- 108102 Influences of hydrogen dilution on microstructure and optical absorption characteristics of nc-SiO<sub>x</sub>:H film**  
Zhao Wei, Du Lin-Yuan, Jiang Zhao-Yi, Yin Chen-Chen, Yu Wei and Fu Guang-Sheng
- 108201 Ion and water transport in charge-modified graphene nanopores**  
Qiu Ying-Hua, Li Kun, Chen Wei-Yu, Si Wei, Tan Qi-Yan and Chen Yun-Fei
- 108202 Surface morphology and electrochemical characterization of electrodeposited Ni–Mo nanocomposites as cathodes for hydrogen evolution**  
Elhachmi Guettaf Temam, Hachemi Ben Temam and Said Benramache
- 108203 Closed-form solution of mid-potential between two parallel charged plates with more extensive application**  
Shang Xiang-Yu, Yang Chen and Zhou Guo-Qing
- 108401 Dual-band LTCC antenna based on 0.95Zn<sub>2</sub>SiO<sub>4</sub>-0.05CaTiO<sub>3</sub> ceramics for GPS/UMTS applications**  
Dou Gang, Li Yu-Xia and Guo Mei
- 108402 Charge and spin-dependent thermal efficiency of polythiophene molecular junction in presence of dephasing**  
Z. Golsanamlou, M. Bagheri Tagani and H. Rahimpour Soleimani
- 108501 Simulation study of the losses and influences of geminate and bimolecular recombination on the performances of bulk heterojunction organic solar cells**  
Zhu Jian-Zhuo, Qi Ling-Hui, Du Hui-Jing and Chai Ying-Chun
- 108502 An improved GGNMOS triggered SCR for high holding voltage ESD protection applications**  
Zhang Shuai, Dong Shu-Rong, Wu Xiao-Jing, Zeng Jie, Zhong Lei and Wu Jian
- 108503 A novel diode string triggered gated-PiN junction device for electrostatic discharge protection in 65-nm CMOS technology**  
Zhang Li-Zhong, Wang Yuan, Lu Guang-Yi, Cao Jian and Zhang Xing
- 108504 Electrical properties of zinc-oxide-based thin-film transistors using strontium-oxide-doped semiconductors**  
Wu Shao-Hang, Zhang Nan, Hu Yong-Sheng, Chen Hong, Jiang Da-Peng and Liu Xing-Yuan
- 108505 A threshold voltage model of short-channel fully-depleted recessed-source/drain (Re-S/D) SOI MOS-FETs with high-*k* dielectric**  
Gopi Krishna Saramekala, Sarvesh Dubey and Pramod Kumar Tiwari
- 108506 Fabrication and characterization of novel high-speed InGaAs/InP uni-traveling-carrier photodetector for high responsivity**  
Chen Qing-Tao, Huang Yong-Qing, Fei Jia-Rui, Duan Xiao-Feng, Liu Kai, Liu Feng, Kang Chao, Wang Jun-Chu, Fang Wen-Jing and Ren Xiao-Min

- 108701 Ultrafast structural dynamics studied by kilohertz time-resolved x-ray diffraction**  
Guo Xin, Jiang Zhou-Ya, Chen Long, Chen Li-Ming, Xin Jian-Guo, Peter M. Rentzepis and Chen Jie
- 108702 Investigation of noise properties in grating-based x-ray phase tomography with reverse projection method**  
Bao Yuan, Wang Yan, Gao Kun, Wang Zhi-Li, Zhu Pei-Ping and Wu Zi-Yu
- 108703 Flexible-reduced field of view magnetic resonance imaging based on single-shot spatiotemporally encoded technique**  
Li Jing, Cai Cong-Bo, Chen Lin, Chen Ying, Qu Xiao-Bo and Cai Shu-Hui
- 108801 Analysis of the interdigitated back contact solar cells: The n-type substrate lifetime and wafer thickness**  
Zhang Wei, Chen Chen, Jia Rui, Sun Yun, Xing Zhao, Jin Zhi, Liu Xin-Yu and Liu Xiao-Wen
- 108802 GaInP/GaAs tandem solar cells with highly Te- and Mg-doped GaAs tunnel junctions grown by MBE**  
Zheng Xin-He, Liu San-Jie, Xia Yu, Gan Xing-Yuan, Wang Hai-Xiao, Wang Nai-Ming and Yang Hui
- 108901 Improved routing strategy based on gravitational field theory**  
Song Hai-Quan and Guo Jin

**GEOPHYSICS, ASTRONOMY, AND ASTROPHYSICS**

- 109201 Spatiotemporal distribution characteristics and attribution of extreme regional low temperature event**  
Feng Tai-Chen, Zhang Ke-Quan, Su Hai-Jing, Wang Xiao-Juan, Gong Zhi-Qiang and Zhang Wen-Yu

JUST FOR AUTHORS  
— CHINESE PHYSICS B